



Gross slip fretting wear performance of a layered thin W-DLC coating: damage mechanisms and life modelling

Title	Gross slip fretting wear performance of a layered thin W-DLC coating: damage mechanisms and life modelling
Author(s)	Leen, Sean B.
Publication Date	2011
Publisher	Elsevier ScienceDirect
Repository DOI	10.1016/j.wear.2010.12.073

Gross slip fretting wear performance of a layered thin W-DLC coating: damage mechanisms and life modelling

A.L. Mohd Tobi^{a,b,*}, P.H. Shipway^a, S.B. Leen^c

^a*Division of Materials, Mechanics and Structures,
University Technology Centre in Gas Turbine Transmission Systems,
University of Nottingham, University Park, Nottingham, NG7 2RD, UK.*

^b*Faculty of Mechanical and Manufacturing Engineering,
Universiti Tun Hussein Onn Malaysia, Batu Pahat, Malaysia.*

^c*Department of Mechanical and Biomedical Engineering, College of Engineering and Informatics,
National University of Ireland, Galway, Ireland.*

Received Date Line

Abstract

Fretting damage, in the form of wear and fatigue-cracking, is a common cause for concern in a wide range of dynamically loaded mechanical joints, and consequently, control of the rates of such damage is commonly addressed either by design or by the choice of materials with enhanced performance. Such material enhancements may be made to the material bulk, or just to the surface regions through surface engineering. In this work, a thin PVD W-DLC coating with a CrN interlayer was deposited onto both a high-strength steel and a titanium alloy. A cylinder-on-flat fretting configuration was employed under gross slip fretting conditions. It was observed that whilst a low coefficient of friction (COF) was measured throughout the wear of the DLC layer, there were variations in the rates of wear which could be correlated with compositional variations within the film. As wear progressed through the carbon-rich and tungsten-rich upper sub-layers of the W-DLC layer, the wear coefficient decreased. With further wear into the CrN underlayer, the wear coefficient and the COF increases. An incremental finite element (FE) wear model based on the Archard wear equation has been used to simulate the coating wear process, with particular emphasis on evolution of the contact geometry for the W-DLC layer. The predicted coating wear life is then shown to correlate, across a range of load-displacement combinations, with a single predictive coating life equation.

Keywords: PVD DLC coating, fretting wear, Finite element model

1. Introduction

* Corresponding author. Tel.: +607 4537702 ; fax: +607 4536080.
E-mail address: abdlatif@uthm.edu.my (A. L. Mohd Tobi)

Fretting occurs when small amplitude relative motion occurs between contacting surfaces and has been identified as leading to significant reduction in service life of a wide range of components through wear or fatigue. Over the last few years there has been tremendous growth in the use of surface coatings to improve wear resistance, reduce surface friction and increase the life of metallic and metallic-based components. The surface coating industry is rapidly changing due to the ever-increasing number of new coatings being produced and the continuous development of new coating processes. Application of a coating which results in a low coefficient of friction (COF) in a contact has been identified as a way to ameliorate fretting fatigue problems [1]. Low friction coatings provide benefits by reducing the magnitude of the applied tangential loading in a displacement-controlled fretting contact configuration and hence reducing the peak stresses at crack nucleation sites [2]. The component life thus increases since the number of cycles needed to nucleate a crack increases. In addition, an increase of hardness of the coated surface may lead to an increase in the wear resistance of surfaces undergoing fretting motion [3, 4].

Diamond-like-carbon (DLC) is the amorphous state of carbon. It is one of the many interesting forms of carbon that has enormous possibilities for practical application and can have properties that rival those of crystalline diamond. DLC coatings are characterised by high hardness and low friction [5]. Golden et al. [1] have shown a significant increase in fretting fatigue life on the application of DLC coatings to Ti-6Al-4V substrates; here, again, the reduction of COF with the application of DLC coating was identified as the factor which increased the fretting fatigue life of the specimen, by reducing the cyclic shear load experienced and its local contact edge stresses. The wear resistance of DLC coating is mainly due to its high hardness which eliminates the adhesive wear and debris transfer in the fretting regime [6].

The doping of DLC coatings with a wide range of different metals has been shown to lead to changes in their mechanical properties (lower internal stress and hardness, improved adhesion) as well as in their tribological properties [7, 8]. However, the inability of DLC coatings to follow the elastic and/or plastic deformation of substrates without failing (brittle fracture) has been a major disadvantage. Indeed, the enhanced tribological performance of DLC coatings can be reduced or even lost on compliant and/or soft substrates such as titanium alloys; it is thus important that DLC coatings have a substrate which has a high load bearing capacity to prevent failure. Dorner et al. [9] have also shown that coating thickness does not change the adherence and resistance against abrasive wear of DLC coatings.

Increases in coating-substrate adhesion, load support ability and wear protection can be achieved by applying intermediate interlayers such as TiN, CrN, and CrAlN on plasma nitrided Ti-6Al-4V substrates [4]. Cr or Ti interlayers have also been used for DLC coatings to increase the adhesion with the substrate [10, 11]. This has also been shown to decrease the wear rate of the DLC coating to that exhibited by the DLC coating alone [5]. It has also been suggested that nitriding of surfaces will provide support for coatings via reduced subsurface deformation, with harder and deeper nitrided layers promoting higher wear resistance of the coatings [4, 5].

In this paper, the gross-slip fretting wear performance of a thin W-DLC coating on two different substrate materials (a high strength steel, known as SCMV, and a titanium alloy, Ti-6Al-4V) was studied. Tests were conducted on a cylinder-on-flat fretting configuration, for different number of cycles, in ambient conditions and

without external lubrication. Images of coating wear scars and their cross-sections provide information on the fretting wear response of the materials. Attention is focused on the tribological performance of the coating as it wears through different sub-layers of the coating and also on the dependency of wear behaviour on substrate material. Furthermore, an FE-based simulation tool for coating wear is presented to allow prediction of coating wear life.

2. Experiments

2.1. Materials and specimens

Fretting wear tests were carried out using a simple laboratory cylinder-on-flat fretting configuration. The flat specimens used in the test have a length of 44 mm, a width of 10 mm and a thickness of 6 mm. The cylindrical specimens are also 44 mm long with the diameter of the half-cylindrical specimen being 12 mm. The substrate materials used in the current study are a high strength steel (SCMV) and a titanium alloy (Ti-6Al-4V), focussed on aeroengine applications where a number of components potentially experience fretting problems such as in the spline coupling [12] and the dovetail fan blade joint [13, 14]. Untreated specimen blanks were manufactured from SCMV and Ti-6Al-4V. The specimen blanks were then heat-treated according to the required specifications and machined to their final dimensions. Coatings were applied to the finished test specimens as appropriate.

SCMV is a high-strength alloy steel based on BS 3S 132:1976 [15], but subjected to a cleaner processing procedure. The test specimens were initially machined slightly oversize from the final required dimension of specimen. These specimens then underwent a two stage heat treatment: an initial heating to 940 °C for 45 minutes followed by an oil quench and final temper at 570 °C for 2 hours with air cooling [16, 17]. Specimens were subsequently ground to size, with a minimum depth of material removal of 0.5 mm to ensure removal of the decarburized layer associated with the heat treatment [16]. After grinding to size, one randomly selected sample was sectioned and a Vickers microhardness profile from the surface to the centre was taken using a 300 gf load. The results confirmed that the decarburised layer was completely removed by the grinding process and a through hardness of 517 HV(0.3) was achieved. The mechanical properties of SCMV have been reported in [2]. For the purpose of the present study, only the elastic properties are considered. The values used are 200 GPa for elastic modulus and 0.3 for Poisson ratio. The microstructural detail of the SCMV specimens was revealed by etching the sample in 2% Nital for ~15 seconds, as shown in Fig. 1. A tempered martensite structure is clearly visible. The specification for the chemical composition of SCMV is shown in Table 1. The surface roughness (Ra) of the test specimens was measured and an average of 5 measurements was taken for the reported value, giving a value of approximately 0.20 µm (Ra).

Ti-6Al-4V is a titanium alloy which is used in the low pressure system of gas turbines, such as the front stub shaft–turbine shaft spline coupling. It is an $\alpha+\beta$ alloy as shown in Fig. 2 [18]. It has a nominal chemical composition of 6 wt% aluminium, 4 wt% vanadium with the remainder being titanium (Table 2). It offers an

excellent combination of low density and high strength, corrosion resistance and strength at moderately high temperatures. The flat and cylindrical fretting specimens were machined from Ti-6Al-4V as-received plates. Before machining, the Ti-6Al-4V had been preheated and solution-treated to achieve moderate increase in strength. This treatment produces a bimodal microstructure. The heat treatment for the test specimen material was as follows:

1. 940°C in vacuum – hold for 2 hours - gas fan quench
2. 900°C in air – hold for 2 hours - air cool
3. 700°C in vacuum – hold for 2 hours - gas fan quench

In order to determine the hardness of the Ti-6Al-4V, Vickers microhardness tests were carried out on one of the specimens. A measurement of 326 HV(0.3) was recorded. The material properties of Ti-6Al-4V have been taken from [18 - 20] and the values are typically reported between 115 and 118 GPa and a Poisson's ratio of 0.34. The surface roughness of Ti-6Al-4V specimens was measured at around 0.20 μm .

2.2. Coating deposition

BALINIT[®] C STAR is a physical vapour deposited (PVD) coating which is made up of a tungsten-containing diamond-like carbon (W-DLC) coating with a chromium nitride (CrN) sub-layer. This coating is produced by Oerlikon Balzers UK Ltd. The vacuum deposition process is operated at a temperature between 180 and 350°C and is intended to achieve a defect-free and homogeneous coating with good adhesive strength. The CrN sub-layer is a hard and relatively tough layer the intended purpose of which is to provide additional load bearing capacity. The W-DLC coating is designed to offer protection against adhesive wear (scuffing) and reduce the risk of surface fatigue and fretting corrosion, via a low coefficient of friction in sliding against a range of materials. The compact CrN layer is intended to enhance the corrosion resistance of the coated component and improve the adhesion of the upper W-DLC coating.

In the present work, both cylindrical and flat specimen surfaces were coated. The surface roughness of the coated components was around $\sim 0.3 \mu\text{m}$ (Ra). The Knoop hardness of the coating layers, as reported by the supplier, are as follows: the top functional layer of the W-DLC has a hardness of 1100 HK (0.01) whilst that of the CrN interlayer is 1750 HK (0.01). Fig. 3 shows a scanning electron microscope back-scattered electron image (SEM-BEI) of a section through the coating, showing the distinct layers in the coating (in total, approximately 4 μm thick). The CrN sub-layer (labelled 2) is the dull section and the W-DLC layer (labelled 3 and 4) is the brighter layer on the surface. The thickness of the top bulk W-DLC layer was measured to be approximately 2 μm (consists of the uppermost W-DLC sub-layer, with a higher carbon concentration of around 1.5 μm thick and the high tungsten layer of around 0.5 μm thick), and approximately 2 μm for the CrN interlayer.

Striations observed within the coating are attributed to changes in the application rates of the constituent elements. The relative brightness is related to the average atomic number of the elements present in a particular phase. For example, directly adjacent to the substrate a slightly brighter band (labelled 1) can be seen. This is due

to a high concentration of chromium. Then, the duller band (2) is indicative of the main bulk of the chromium-nitride layer. A similar composition to (1) is seen before the transition to the most noticeable bright seam (3) which has the highest concentration of tungsten; the upper band (4) is duller due to a greater concentration of carbon in the W-DLC.

2.3. Fretting tests

Fretting motion was applied in a displacement controlled manner by an oscillatory vibrator with a constant normal load applied with a dead-weight using a simple laboratory cylinder-on-flat fretting configuration (Fig. 4). A linear variable displacement transducer (LVDT) was used to continuously measure the applied displacement and strain gauges were used to measure the tangential traction forces throughout the tests. The frequency of vibration in all of the fretting tests was kept constant at 20 Hz. A real time signal control and data acquisition system was used to characterise and evaluate the frictional response. The fretting test rig setup is schematically illustrated in Fig. 5. All tests were of similar pairs of flat and cylindrical specimens (i.e. like-on-like). The specimen pairs were fretted against each other under a specific applied normal load with an applied displacement for a predetermined number of fretting cycles. The fretting conditions investigated in this study are summarised in Table 3.

2.4. Assessment of wear surfaces

The surface wear profile following each test was evaluated using profilometry. At this stage, loose debris on the specimen was removed by compressed air while the compacted debris remained. All of the wear scars on the flat specimen were analysed using a Taylor-Hobson Talysurf CLI 1000 with a fine diamond stylus (2 μm radius) to evaluate the shape and depth of the wear scars produced. An area of 2.5 mm \times 8 mm was profiled over each wear scar. The scan produced 401 profiles individual line with 20 μm spacing. Readings along each profile were taken at 1 μm intervals. The data were analysed using the accompanying software – Talymap Universal. This allowed each scan to be levelled and a mean profile to be extracted to give a better representation of the wear scar shape. Additionally, the severity of wear could be calculated from the volume of the scar. This was evaluated by calculating the worn area from the average wear profiles height $h(x)$ using Simpson's rule and multiplying by the width of the flat specimen, b . The flat specimen experimental wear volume, V_{exp} , can be expressed as follows,

$$V_{exp} = b \int_{-W/2}^{W/2} h(x) dx \quad (1)$$

where W is the wear scar width. Post-test examination of the wear scars was carried out by SEM and optical microscopy to identify the dominant wear and damage mechanisms. The specimens that required sectioning were cut on a diamond wheel, mounted and polished. Optical microscopy was initially used to take plan view images of the wear scars. Information on surface topography was gained from the SEM secondary electron images (SEI)

whilst the SEM-BEI images provided information on element distribution on the specimen cross sections. Further chemical characterization was achieved using energy dispersive X-ray (EDX) analysis with a beam energy of 10 keV.

3. Experimental results

3.1. Hysteresis loop

The fretting tests exhibited hysteresis loops representative of gross slip conditions for both the coated SCMV and Ti-6Al-4V substrates. Fig. 6a shows hysteresis loops of the coated SCMV pair up to 600,000 cycles. A maximum tangential force of around 175 N was observed at 100,000 cycles before loop stabilisation, with a maximum tangential force of 150 N observed at the end of 300,000 and 600,000 cycles. For the Ti-6Al-4V substrate, tests for up to 300,000 cycles exhibited similar behaviour to the SCMV substrates. However, as shown in Fig. 6b, with further cycling up to 600,000 cycles, a change in shape of the hysteresis loop was observed; specifically, the loop became narrower and taller with a maximum tangential force of approximately 220 N.

3.2. Coefficient of friction

The evolutions of COF up to 600,000 cycles for the coated SCMV and Ti-6Al-4V substrates are shown in Fig. 7. The coated SCMV specimens exhibited a stabilised COF of about 0.3 following a small decrease from a value of 0.35 at 200,000 cycles. For the Ti-6Al-4V specimens, a stabilised value close to 0.3 was observed up to around 300,000 cycles before it increased, in almost step-wise fashion, to ~ 0.5 up to 600,000 cycles.

3.3. Wear profile

Fig. 8a shows the 2-D average worn surface profiles of the coated SCMV flat specimens for 100,000, 300,000 and 600,000 fretting cycles. A 'U-shaped' wear scar was observed at the end of 100,000 cycles with a maximum wear depth of $\sim 1.2 \mu\text{m}$ at the centre of the wear scar. The coated SCMV pairs tested up to 300,000 and 600,000 cycles exhibited a 'W-shaped' wear scar with maximum wear depths of $2 \mu\text{m}$ and $2.5 \mu\text{m}$, respectively.

Fig. 8b shows the 2-D average worn surface profiles of the coated Ti-6Al-4V specimens. At the end of 100,000 cycles, the maximum wear depth was $\sim 1.5 \mu\text{m}$. A 'W-shaped' wear scar with a maximum wear depth of $\sim 2 \mu\text{m}$ was recorded after 300,000 cycles. A maximum wear depth to $3.2 \mu\text{m}$ was obtained after 600,000 cycles. The wear scar of the coated Ti-6Al-4V specimen after 600,000 cycles is significantly larger than in the coated SCMV specimen under the same conditions. Although the 600,000 cycle wear depths for the coated Ti-6Al-4V specimens are found to approach the coating thickness, complete wear through the coating did not occur for any

of the cases studied here. It should be noted that all maximum wear depths recorded are smaller than the overall coating thickness (4 μm).

The wear volumes measured from all the wear scars shown in Fig. 8 are presented as a function of number of cycles in Fig. 9. It can be seen that the wear volumes of the coated Ti-6Al-4V substrates are larger than those of the coated SCMV substrates. At 600,000 cycles, the wear volume difference between the SCMV and Ti-6Al-4V specimens is significantly higher than at the end of 100,000 and 300,000 cycles. The wear rate for the first 100,000 cycles (primary wear rate $\sim 1.1 \times 10^{-6} \text{ mm}^3/\text{Nm}$) was found to be higher than that during the remaining cycles (secondary wear rate $\sim 1.3 \times 10^{-7} \text{ mm}^3/\text{Nm}$) as shown in Fig. 9. The primary wear rate recorded is found to be similar to the wear rate of DLC coatings reported in the literature [7, 8, & 21].

3.4. Microscopy of the wear scars

Figs. 10a and 10b show plan view SEM-BEI wear scar images of the coated SCMV flat specimen after 300,000 wear cycles. A scar width of around 0.5 mm is observed, which agrees with the corresponding 2-D wear profiles (Fig. 8a). The variable contrast levels on the SEM-BEI images suggest different surface material compositions (Fig. 8a). Fig. 8b shows a higher magnification image from location 'A' of Fig. 8a, indicating the locations from which EDX analyses were taken. The EDX analyses confirmed the presence of significant levels of both chromium and tungsten in the S1 region, while only chromium was indicated in the S2 region. EDX analysis on region S3 indicates the presence of W-DLC coating in that region with a high tungsten count and only very small levels of chromium. No traces of iron were found at any of the EDX locations.

Figs. 11a to 11c show SEM-BEI cross-section images of the coated SCMV flat specimen after 100,000, 300,000 and 600,000 cycles, respectively. After 100,000 cycles, the wear is confined within the bulk W-DLC layer, which is still intact on top of the high tungsten layer. In Fig. 11b, the bulk W-DLC layer has almost worn through after 300,000 cycles. After 600,000 cycles, Fig. 11c shows that the coating has worn through the high tungsten layer with only traces of it left on the CrN layer.

Fig. 12 shows the SEM-BEI plan view of the coated Ti-6Al-4V substrate flat specimen following 300,000 wear cycles. A wear scar of about 0.6 mm in width can be observed with debris scattered at the edges. A bright region (high tungsten) is observed across most of the area within the wear scar with small darker patches. Fig. 12b shows a higher magnification image of location 'A' in Fig. 12a. EDX analyses were carried out on the locations shown in Fig. 12b. Significant amounts of tungsten and chromium was detected in the S1 region. Results on the region S2 indicate high levels of chromium with no evidence of significant tungsten and the S3 region show only high tungsten levels with an absence of chromium. There is no evidence for any substrate elements in the EDX analyses conducted.

Figs. 13a to 13c show the SEM-BEI cross-section images of the coated Ti-6Al-4V substrates after 100,000, 300,000 and 600,000 cycles, respectively. At the end of 100,000 cycles, most of the bulk W-DLC layer has been worn away, but a continuous layer remains (Fig. 13a). After 300,000 cycles, the cross-section image shows that the high tungsten layer has been removed with significant areas where the CrN layer has been exposed (Fig. 13b).

Fig. 13c shows that after 600,000 cycles the coating has worn through the CrN sub-layer, with a substantial level of cracking of this layer also being observed.

4. Computational model

4.1. Incremental wear simulation method

The geometry evolution of the contact due to wear is modelled using a modified version of the Archard wear model, as previously described in [22 – 24]. It is briefly outlined here for completeness. A modified Archard equation (the modification referred to here is the implementation of the Archard equation on a local, pointwise basis, in terms of nodal contact pressures and relative slips, as opposed to the original global basis, in terms of normal load and distance slid), defining the incremental wear depth Δh for a specific point x experiencing an incremental slip $\delta(x,t)$ and pressure $p(x,t)$ at specific time t , is given as:

$$\Delta h(x,t) = k_1 p(x,t) \delta(x,t) \quad (2)$$

where k_1 is the ‘local’ wear coefficient, expressed as the wear per unit local slip per unit local contact pressure which can typically be expected to depend on a number of variables, including slip, pressure, number of cycles. It is not presently possible to measure k_1 . Consequently, the approach adopted here is to use an average wear coefficient, k , which can be determined from the measured wear scar [22] using the following equation:

$$k = \frac{V_{\text{exp}}}{4\delta_{\text{actual}} \times N_t P} \quad (3)$$

where N_t is the total number of fretting cycles. The V_{exp} term is the estimated total wear volume of the flat specimen (from Eq. 1). Since modelling each individual cycle would be computationally expensive, a cycle jump technique has been used, following the method of [22]. This technique applies the wear corresponding to a cycle jump of ΔN cycles incrementally during one (simulated) fretting cycle:

$$\Delta h(x,\tau) = \Delta N k p(x,\tau) \delta(x,\tau) \quad (4)$$

where τ is time increment within one cycle corresponding to ΔN wear cycles.

Wear by the modified Archard equation is implemented in the analysis using an adaptive mesh technique implemented via the UMESHMOTION user subroutine within ABAQUS (Version 6.7). The adaptive meshing algorithm of ABAQUS applies the local wear increment for all surface nodes in two steps. First, the local wear increment is implemented by moving the surface nodes in the local normal direction; this geometry update is implemented as a purely Eulerian analysis (Fig. 14a). Secondly, the material quantities (variables) are re-mapped to the new positions by advection from the old location to the new location by solving the advection equations using a second order numerical method called the Lax-Wendroff method [25]. The adaptive meshing algorithm is only applied to the elements in the coating, viz. not to the coating-substrate interface or below, to ensure that the interface boundary between the coating and the substrate is preserved during the wear simulation.

Due to the non-linear behaviour of the contact analyses and the incremental nature of the applied wear model, the time domain in one analysis step was divided into a number of small increments. 50 increments per tangential displacement step and 100 increments per cycle were found to be satisfactory to maintain solution stability and accuracy as discussed in detail by Madge [26]. For the current work, a cycle jump value, ΔN of 2000 has been used. Since the wear model updates the surface profile for every increment in a step, the effect of ΔN on the wear solution stability and accuracy in terms of the wear profile and stress distribution were found to be acceptable for these values [26]. However it is important to note that the solution stability and accuracy depend on all the parameters which define the incremental wear depth i.e. the wear coefficient, the slip experienced, the contact loading and the cycle jump value used. For example, in wear of a contact which exhibits a high wear coefficient with a high applied slip, smaller ΔN values are required to maintain solution stability and accuracy.

In order to simulate up to 600,000 cycles, it was necessary to develop a new Python scripting framework, as illustrated in the flowchart of Fig 14b. Specifically, this circumvented CPU limitations whereby 100,000 cycle simulations could be carried out in UMESHMOTION and results passed via the Python code to generate a new analysis for the next 100,000 cycle simulation. Thus, the Python framework facilitates a sufficiently refined time (ΔN) and spatial discretisation for significantly larger numbers of wear cycles, even exceeding 600,000 cycles, for example.

The purpose of the wear modelling is to develop and validate a predictive model for coating wear life across different fretting conditions (load-displacement combinations) based on identification of empirical constants from a representative pair of tests. The approach adopted in the present work is a first step towards modelling of fretting wear in coatings and employs a number of simplifying assumptions with respect to tribological and mechanical properties of the coating, as follows:

1. The coating is represented as a perfectly adhered single layer which is assumed to have a thickness equal to the combined thickness of all four sub-layers identified in Fig. 3.
2. The elastic properties of the coating are assumed to be homogeneous, despite the detailed observations about the complex sub-layer composition of the present coating presented above
3. The COF of the coating is assumed to remain constant, i.e. with respect to wear depth, number of cycles.
4. The wear coefficient of the coating is assumed to follow a bilinear response, as shown in Fig. 9, whereby the primary wear coefficient corresponds to sub-layer 4 of Fig. 3, i.e. the uppermost W-DLC sub-layer, with a higher carbon concentration, while the secondary wear coefficient corresponds to sub-layer 3 of Fig. 3, i.e. the high tungsten layer.
5. For simplicity, the residual stresses which normally occur in coatings due to the deposition process are not modelled.
6. Wear debris and so-called third-body effects are not included in the model.

Future work will investigate the identification of the elastic properties of the different sub-layers. However, previous wear simulation analyses by the authors [27], across different values of coating elastic modulus, have shown that the effect of elastic modulus is not a first order effect in coating wear profile evolution.

Since similar failure behaviour was observed in tests on both coated SCMV and Ti-6Al-4V substrates and more stabilised wear behaviour was observed for the coated SCMV test (Fig. 9), only the coated SCMV pair wear was simulated. The primary wear coefficient of $1.1 \times 10^{-6} \text{ mm}^3/\text{Nm}$ was employed up to 100,000 fretting cycles and the additional 500,000 fretting cycles being simulated employed a secondary wear coefficient of $1.3 \times 10^{-7} \text{ mm}^3/\text{Nm}$ up to 600,000 fretting cycles. The number of cycles demarcating this change in wear coefficient (100,000 cycles) was identified from Fig. 9 and the observed cross sectional images of the coated SCMV for 100,000, 300,000, and 600,000 cycles (Fig. 11). It was estimated that the coated SCMV wear coefficient changed at the end of $\sim 100,000$ cycles, corresponding to when it started to wear through into the high tungsten layer. The wear coefficient applied is assumed to be an average across both contacting surfaces.

4.2. FE model

The elastic material constants assumed for the SCMV substrate are a Young's modulus, E_s , of 200 GPa and a Poisson's ratio of 0.3. Substrate plasticity was evaluated using the von Mises yield criterion and it was established that plasticity is not predicted for the SCMV substrate. A coating elastic modulus of 100 GPa [10, 28] and Poisson's ratio of 0.2 was assumed for the coating [29]. Coulomb friction is employed based on the Lagrange multiplier contact algorithm to ensure an exact stick condition when the shear stress is less than the critical shear value, according to the Coulomb friction law. A COF of 0.3 was assumed on the contact surfaces, based on the measured stabilised gross slip values (Fig. 7).

Further details of the contact modelling methodology employed here are given in [27]. A normal load and applied displacement of $P = 500 \text{ N}$, $\delta^* = 20 \text{ }\mu\text{m}$ (observed from the test) were applied to the top surface of the cylinder while constraining the bottom half of the flat specimen in the x and y -directions.

Figs. 15a and 15b show the FE models of the coated cylinder-on-flat fretting specimens. The element dimensions in the coating layer and on the contact surfaces are $4 \text{ }\mu\text{m}$ square, i.e. the coating is modelled as a single layer of elements. A sharp transition from the fine mesh region (on the contact surfaces) to the coarser mesh (further from the contact) gives a high degree of accuracy for the predicted stress field. Detailed mesh size studies presented by the authors [27] show that, for the $4 \text{ }\mu\text{m}$ coating thickness, a single layer of $4 \text{ }\mu\text{m}$ thick elements agrees, to within 10%, in terms of stress distributions, with a 4-layer mesh of $1 \text{ }\mu\text{m}$ thick elements. The benefit of the thicker elements, however, is reduced CPU times and memory requirements, particularly for incremental wear simulations.

The full width of coating was not modelled, as shown schematically in Fig. 15c; however, the width of coating modelled (1.2 mm) was, (as shown below) more than double the final wear scar width; comparative FE studies have established that the contact (surface and sub-surface) stresses in the coating regions of interest are

unaffected by this simplification. This also helped with respect to reducing the computational overhead of the wear simulations, particularly when combined with the optimised mesh design. The present FE modelling methodology was successfully validated against the analytical solutions of Gupta et al. [30] and Gupta & Walowit [31] for a cylindrical indenter on a layered substrate, with respect to both contact pressure and interface stresses in [27].

5. FE Results

5.1. Predicted wear profile

Fig. 16 shows the comparison of the FE predicted wear profile and experimentally measured wear profiles for the coated SCMV substrates after 100,000, 300,000 and 600,000 cycles. All the FE predicted wear volumes are within 90% of the experimental wear volume. The model consistently predicts a 'U shaped' evolving wear scar geometry, which give reasonable correlation with the measured profile for 100,000 cycles. The measured profiles for greater than 300,000 cycles are characterised by a 'W-shaped' wear scar. This shape is attributed to the effects of wear debris and the associated third body effect, which is not included in the present modelling methodology.

Fig. 17 shows a comparison of the FE-predicted and experimentally-observed maximum wear depths as a function of number of cycles, against a background (at the correct scale) of the original coating cross-section image for the coated SCMV pair. The predicted and measured results show good agreement, both in terms of the maximum values and the bilinear wear rate transition. The predicted wear depth from the primary wear period at the end of 100,000 cycles is around 1.4 μm which is close to the thickness of the carbon-rich W-DLC layer, sub-layer 4 of Fig. 3. After 600,000 cycles (with secondary wear rate effects), the predicted wear depth increased to 2 μm depth, corresponding to the depth of the interface between the high tungsten concentration W-DLC (sub-layer 3 in Fig. 3). The secondary wear simulation is seen to slightly under-predict maximum wear depth, although the primary wear simulation slightly over predicts.

6. Discussion

6.1. Coating performance

A low COF of around 0.3 was observed in both fretting of coated SCMV and Ti-6Al-4V substrates as the coating was worn through the bulk W-DLC layer and high tungsten concentration layer. This can be seen by comparing the COF evolution with cycles (Fig. 7) with the cross sectional images of the wear scars at the end of the tests (Figs. 11 and 13). The increase in COF for the coated Ti-6Al-4V test to around 0.5 just after 300,000 cycles (Fig. 7) corresponds to the total loss of the W-DLC layers and thus to the fretting of the CrN layer in the

couple. Evidence for this can be seen from the specimen cross section image following 300,000 and 600,000 cycles of wear (Fig. 13).

From the plan view images of the wear scar and EDX analyses conducted for the coated SCMV at the end of 300,000 cycles, there is evidence of CrN on the wear scar surface (the darker grey material of type S2 shown in Fig. 10). However, since most of the worn surface was still covered by bulk W-DLC layer (the mid-grey material of type S3 shown in Fig. 10), the coating still exhibited a low COF. For the coated Ti-6Al-4V at the end of 300,000 cycles, the plan view shows that most of the surface was comprised of the high tungsten concentration layer (the bright material of type S1 shown in Fig. 12) with some regions where CrN had been exposed (the darker grey material of type S2 shown in Fig. 12). Once the CrN was exposed over most of the surface, the COF increased, which occurred slightly after 300,000 cycles (Fig. 7). Furthermore, the increase in COF is a possible reason for the presence of cracking within the CrN layer following the 600,000 cycles test (Fig. 13c). The increase in COF leads to higher traction stresses being imposed on the coating and may have induced tensile fracture within the coating [32]. In contrast to similar tests on both uncoated SCMV and Ti-6Al-4V substrates where subsurface cracking was observed [33], no substrate cracking was observed in any of the tests, suggesting the beneficial effects of both low COF and gross slip wear-induced stress reduction.

From the tests, it was also found that two broad regimes of behaviour, with very different rates of wear were observed as the coating wore through its thickness (Fig. 9). Comparing these with the cross section images (Figs. 11 and 13) of the specimens, it was found that the change of wear coefficient corresponded to wear-induced progressive exposure of the different layers of coating. For the SCMV substrate for example, the specimen cross section at the end of 100,000 cycles (where the primary wear rate was applicable) shows that the coating has not worn through the bulk W-DLC coating (Fig. 11a). However, cross sectional images of wear scars following 300,000 and 600,000 cycles show the coating has started to wear into the high tungsten concentration layer (Figs. 11b and 11c), for which the secondary wear rate is applicable. Therefore, it can be concluded that the primary wear rate is associated with wear in the bulk W-DLC layer and the secondary wear rate is associated with wear within the high tungsten concentration layer. The significant increase in wear volume at the end of 600,000 cycles for the coated Ti-6Al-4V substrate (Fig. 9) suggests an increase in wear rate as the coating wore through into the CrN layer, as seen from the cross section on Fig. 13c.

The fretting tests indicate that the wear resistance of the coating on the SCMV substrate is higher than that on the Ti-6Al-4V substrate. The SCMV is a harder and stiffer substrate than Ti-6Al-4V and this increases the coating load support and thus reduces subsurface deformation (elastic and/or plastic) and improves uniformity of strain distributions. This will lead to reduction of coating strain along with the possibility of damage or cracking of the brittle coating. The effect of substrate type on the coating wear rate has also been observed by a number of other workers. Meletis et al. [5] presented pin-on-disc sliding wear tests of Al_2O_3 pins on DLC coated Ti-6Al-4V and M50 steel substrates and showed that the wear rate of the DLC coated M50 steel substrate was lower than that of the DLC coated Ti-6Al-4V substrate. Further they also showed that plasma nitriding the substrate increased the wear resistance of the DLC coating compared to a non-nitrided/DLC coated substrate. Similar results have also been obtained by Jiaren et al. [34] from sliding wear tests using tungsten carbide balls on a range of DLC-coated

substrates (steels and aluminium alloys) where they found that the wear resistance of the coating increased with increasing substrate hardness. Takadoum et al. [35] conducted alumina sphere-on-disc sliding wear testing of TiN, TiCN and DLC coatings on two steel substrates with different hardnesses (250 and 880 HV) and again, they showed that the wear resistance of all the coatings were higher on the harder substrate. Furthermore, fretting wear tests of TiN coated cylinder-on-flat (6 mm radius of cylinder) specimens with different substrates (ferrous alloys with hardness of 188 to 674 HV, Ti-6Al-4V and an aluminium alloy ASCM20) conducted by Shima et al. [36] also showed similar behaviour.

Therefore, it can be concluded that both the stiffer and harder substrate are beneficial for coating load support. A stiffer substrate will reduce the subsurface elastic deformation whilst a harder substrate will reduce plastic deformation either by gross plasticity or by the local plastic deformation of the substrate [36]. By reducing the deformation of the coating in this way, the probability of coating damage will thus be reduced.

The measured transition of wear scar shape from a ‘U-shape’ to a ‘W-shape’ as wear progresses (Fig. 8) is probably due to the third body debris effect in the contact; this effect is not included in the present model. The changes in the competition between debris formation and debris rejection during fretting may contribute to this. As the wear continues, the contact becomes conforming and the contact surface becomes wider which will influence the debris ejection process. The trapped debris may increase the wear rate in some locations, creating the ‘W-shaped’ wear scar as wear progresses. Fouvry et al. [37, 38] observed a similar ‘W-shaped’ wear scar morphology following fretting testing of an alumina ball on TiN-coated high speed steel substrates. They argued that oxidised debris transferred onto the alumina ball and that this transferred material then created a high contact pressure region which increased the wear rate in that region on the coating and created a ‘W-shaped’ wear scar. However, in the current work, no evidence of any material transfer was found on the cylindrical counter-part when viewed under the SEM, suggesting that this mechanism does not account for the ‘W-shaped’ scar in this case. The implementation of a debris layer wear simulation method, such as that presented in [39, 40], could possibly improve the prediction of wear scar shape. However, the debris layer simulation model requires both the mechanical properties of the debris layer itself and also the development of a complex plastic-strain assisted oxidation wear model [41] for the materials in question, and as such, is not a trivial task to apply to the DLC coating system being considered.

6.2. Coating life prediction

The wear simulation on the coated SCMV substrate shows that the predicted maximum wear depth coincides well with the different layer thicknesses within the coating (Fig. 17). For a given wear coefficient, FE simulations are able to predict the wear depth. Therefore, for a coating under gross slip fretting conditions, assuming a low risk of tensile fracture and good coating adhesion [27], the service life of a coating can be based on the progression of wear depth. Fig. 18 shows the FE-predicted evolution of coated SCMV wear depth (primary wear rate) for the following range of normal load, applied displacement combinations: (i) $P = 350$ N, $\delta^* = 20$ μm , (ii) $P = 500$ N, $\delta^* = 20$ μm , and (iii) $P = 700$ N, $\delta^* = 60$ μm . The ratio of the wear depth, h to the coating thickness

from test, t_c is presented on the y -axis. The independent parameter in Fig. 18 is the ratio of the product of normal load and total sliding distance ($4 \times P \times \delta^* \times N$) to the product of normal load and total sliding distance from fretting test of BCS-coated SCMV with $P = 500$ N, $\delta^* = 20$ μm up to 100,000 cycles, $(4 \times P \times \delta^* \times N)_{\text{test}}$. It can be seen that all of the ratio of the predicted wear depth to coating thickness from test, h/t_c , for different normal load and applied displacement, represented by different values of $(4 \times P \times \delta^* \times N)/(4 \times P \times \delta^* \times N)_{\text{test}}$, lie close to the best fit trend for the $P = 500$ N, $\delta^* = 20$ μm case. Thus, it is clear that, for these cases at least, identification of the empirical constants for the relationship plotted in Fig. 18 from one set of test conditions, permits prediction of the evolution of wear depth for other test conditions, for the same configuration and contact condition. The equation for the trendline in Fig. 18 is as follows:

$$N_h = \frac{0.71 \sqrt{\frac{h/t_c}{0.364}} \times (4 \times P \times \delta^* \times N)_{\text{test}}}{4 \times P \times \delta^*} \quad (5)$$

where h/t_c is the ratio of required wear depth to the coating thickness, N_h is coating wear-life for a depth h , P is the applied normal load (in N) and δ^* is applied displacement, where δ^* is the same as δ_{actual} from the tests (in mm).

There are three important points in relation to the model and predictive method presented here. One is that, although the modified Archard wear model has limitations, typically wear volume information is only required from one or two ‘representative’ tests in order to be able to predict across a range of load and displacement conditions. This has been established in a number of previous publications for non-coated substrates, e.g. [16], [22] and is shown here for a coated substrate in Fig. 18. The second point is that the benefits of a wear model are that it can give additional information to that available experimentally. Specifically, it can provide valuable information about (i) the evolutions of stresses and strains in the coating itself, e.g. see [27], (ii) the evolutions of stresses and strains in the substrate, e.g. [33], (iii) the effects of key coating design variables not easily modified (at least systematically) in experiments and thus, perhaps most importantly, ultimately (iv) the ability to design coatings for specific tribological requirements. Finally, of course, a key benefit of an FE-based wear model is the possibility to investigate, at least computationally, the performance of coatings in complex geometry applications, e.g. real three-dimensional applications such as dovetail joints [14] and spline couplings [12].

A similar approach has been presented based on the energy wear approach in [38, 42, 43] to quantify fretting contact durability of a coating. A contact wear endurance curve was presented, in which the global endurance (number of cycles to substrate exposure) of the coated systems investigated could be assessed from its mean contact energy density.

The coating life prediction approach presented here is applicable to a stabilised gross slip condition for a given contact configuration; changing configuration or slip regime may change the rates and mechanisms of wear. Further work is needed to verify this. Although some important effects have been neglected, specifically, (i) inhomogeneity of the coating with respect to sub-layers and associated mechanical and tribological properties, (ii) residual stress from the deposition process and (iii) third body (debris) effects, it is intended to address these effects in future work, based on previous work in [39, 40, 44]. A key next step for the design of coatings must be the development of a multi-layer coating wear methodology.

Clearly, different interacting modes of coating failure exist and must be designed against. Thus, this paper is concerned with modelling wear in coatings. An additional consideration is that brittle (coating) fracture, if it occurs, will occur in the early cycles [27], so that the present work basically assumes that brittle fracture has not occurred and hence failure by wear or shear delamination needs to be evaluated. Also, the present work does not make any specific assumption about the mode of (asperity) fracture associated with wear.

7. Conclusions

Experimental testing of a layered W-DLC coating on SCMV and Ti-6Al-4V substrates has been employed to identify the tribological behaviour of the coating. Coating wear life can (in certain circumstances) be predicted in terms of maximum wear depth and based on a simplified coating model. The following conclusions can be made from the fretting testing and analyses of the coated substrates:

- No gross coating failure (by delamination etc.) was observed under the gross slip conditions examined in this work.
- The wear resistance of the coating on the SCMV substrate was higher than that on the Ti-6Al-4V substrate due to higher load bearing capacity of the SCMV substrate.
- A low COF of 0.3 was observed for the W-DLC layer and a higher COF of 0.5 for the CrN underlayer.
- Within the W-DLC layer, the high tungsten concentration layer exhibited greater wear resistance than the bulk W-DLC coating. The wear rate increased as the coating reached the CrN layer.
- No cracking was observed as the coating wore through the W-DLC layer, but cracking of the coating was observed as the coating reached the CrN layer. The increase in COF may contribute to this behaviour.
- The wear scar evolved from 'U-shaped' geometry for less than 100,000 cycles to a 'W-shaped' wear scar for higher numbers of cycles. This may be attributed to third body debris effects.
- Change of wear behaviour for different layers within the coating can be modelled by changing the wear coefficient within the FE wear model. The predicted wear depth agrees well with the test results.
- A parameter consisting of normal applied load and total sliding distance can be used to predict the coating wear life based on worn coating thickness.

Acknowledgements

The authors wish to thank Rolls-Royce plc, Aerospace Group, for their financial support of the research, which was carried out at the University Technology Centre in Gas Turbine Transmission Systems at the University of Nottingham. The views expressed in this paper are those of the authors and not necessarily those of Rolls-Royce plc, Aerospace Group. We also would like to thank Oerlikon Balzers UK Ltd and Dr Spyros Katsikis for their technical support and providing BALINIT[®] C STAR coating for the research.

References

- [1] P.J. Golden, A. Hutson, V. Sundaram, J.H. Arps, Effect of surface treatments on fretting fatigue of Ti-6Al-4V. *International Journal of Fatigue* 29 (2007) 1302-1310.
- [2] S.B. Leen, I.J. Richardson, I.R. McColl, E.J. Williams, T.R. Hyde, Macroscopic fretting variables in a splined coupling under combined torque and axial load. *Journal of Strain Analysis for Engineering Design* 36 (2001) 481-497.
- [3] E. Spain, J.C. Avelar-Batista, M. Letch, J. Housden, B. Lerga, Characterisation and applications of Cr-Al-N coatings. *Surface and Coatings Technology* 200 (2005) 1507-1513.
- [4] J.C. Avelar-Batista, E. Spain, G.G. Fuentes, A. Sola, R. Rodriguez, J. Housden, Triode plasma nitriding and PVD coating: A successful pre-treatment combination to improve the wear resistance of DLC coatings on Ti6Al4V alloy. *Surf. Coat. Technol.* 201 (2006) 4335-4340.
- [5] E.I. Meletis, A. Erdemir, G.R. Fenske, Tribological characteristics of DLC films and duplex plasma nitriding/DLC coating treatments. *Surface and Coatings Technology* 73 (1995) 39-45.
- [6] M. Kalin, J. Vizintin, The tribological performance of DLC coatings under oil-lubricated fretting conditions. *Tribology International* 39 (2006) 1060-1067.
- [7] M. Sedlacek, B. Podgornik, J. Vizintin, Tribological properties of DLC coatings and comparison with test results: Development of a database. *Materials Characterization* 59 (2008) 151-161.
- [8] C.W. Moura e Silva, J.R.T. Branco, A. Cavaleiro, How can H content influence the tribological behaviour of W-containing DLC coatings. *Solid State Sciences* 11 (2009) 1778-1782.
- [9] A. Dorner, C. Schürer, G. Reisel, G. Irmer, O. Seidel, E. Müller, Diamond-like carbon-coated Ti6Al4V: influence of the coating thickness on the structure and the abrasive wear resistance. *Wear* 249 (2001) 489-497.
- [10] J.S. Wang, Y. Sugimura, A.G. Evans, W.K. Tredway, The mechanical performance of DLC films on steel substrates. *Thin Solid Films* 325 (1998) 163-174.
- [11] C. Wei, J.-Y. Yen, Effect of film thickness and interlayer on the adhesion strength of diamond like carbon films on different substrates. *Diamond and Related Materials* 16 (2007) 1325-1330.
- [12] S.B. Leen, T.H. Hyde, C.H.H. Ratsimba, E.J. Williams, I.R. McColl, An investigation of the fatigue and fretting performance of a representative aero-engine spline coupling. *Journal of Strain Analysis for Engineering Design* 37 (2002) 565-583.
- [13] M. Ciavarella, G. Demelio, A review of analytical aspects of fretting fatigue, with extension to damage parameters, and application to dovetail joints. *Int. J. Solids Struct.* 38 (2001) 1791-1811.
- [14] R. Rajasekaran, D. Nowell, Fretting fatigue in dovetail blade roots: Experiment and analysis. *Tribology International* 39 (2006) 1277-1285
- [15] British Standards Institution, BS 3S 132:1976, Specification. 3% chromium-molybdenum-vanadium steel billets, bars, forgings and parts (1320-1470 MPa: limiting ruling section 70 mm) (suitable for nitriding), British Standards Institution, 1976.
- [16] J. Ding., Modelling of fretting wear, PhD Thesis, University of Nottingham, 2003.
- [17] H.P. Soh., Fretting wear studies of aeroengine materials, PhD Thesis, University of Nottingham, 2006.
- [18] D. Eylon, Summary of the Available Information on the Processing of the Ti-6Al-4V HCF/LCF Program Plates, University of Dayton, Dayton, Ohio, 1998
- [19] R.J. Morrissey, D.L. McDowell, T. Nicholas, Frequency and stress ratio effects in high cycle fatigue of Ti-6Al-4V. *International Journal of Fatigue* 21 (1999) 679-685.
- [20] J.A. Araújo, D. Nowell, The effect of rapidly varying contact stress fields on fretting fatigue. *International Journal of Fatigue* 24 (2002) 763-775.
- [21] S.J. Bull, Tribology of carbon coatings: DLC, diamond and beyond. *Diamond and Related Materials* 4 (1995) 827-836.
- [22] I.R. McColl, J. Ding, S.B. Leen, Finite element simulation and experimental validation of fretting wear. *Wear* 256 (2004) 1114-1127.

- [23] J. Ding, S.B. Leen, I.R. McColl, The effect of slip regime on fretting wear-induced stress evolution. *International Journal of Fatigue* 26 (2004) 521-531.
- [24] J.J. Madge, S.B. Leen, I.R. McColl, P.H. Shipway, Contact-evolution based prediction of fretting fatigue life: Effect of slip amplitude. *Wear* 262 (2007) 1159-1170.
- [25] Abaqus User's Manual, Version 6.7. RI, US: HKS Inc.; 2007.
- [26] J.J. Madge., Numerical modelling of the effect of fretting wear on fretting fatigue, PhD Thesis, University of Nottingham, 2008.
- [27] A.L. Mohd Tobi, J. Ding, S. Pearson, S.B. Leen, P.H. Shipway, The effect of gross sliding fretting wear on stress distributions in thin W-DLC coating systems. *Tribology International* 43 (2010) 1917-1932.
- [28] N. Yao, A.G. Evans, C.V. Cooper, Wear mechanism operating in W-DLC coatings in contact with machined steel surfaces. *Surf. Coat. Technol.* 179 (2004) 306-313.
- [29] R. Wang, C. Mercer, A.G. Evans, C.V. Cooper, H.K. Yoon, Delamination and spalling of diamond-like-carbon tribological surfaces. *Diamond and Related Materials* 11 (2002) 1797-1803.
- [30] P.K. Gupta, J.A. Walowit, E.F. Finkin, Stress distributions in plane strain layered elastic solids subjected to arbitrary boundary loading. *Journal of Lubrication Technology-Transactions of the Asme* 95 (1973) 427-433.
- [31] P.K. Gupta, J.A. Walowit, Contact stresses between an elastic cylinder and a layered elastic solid. *Journal of Lubrication Technology-Transactions of the Asme* 96 (1974) 250-257.
- [32] K. Holmberg, A. Laukkanen, H. Ronkainen, K. Wallin, Tribological analysis of fracture conditions in thin surface coatings by 3D FEM modelling and stress simulations. *Tribology International* 38 (2005) 1035-1049.
- [33] A.L. Mohd Tobi, J. Ding, G. Bandak, S.B. Leen, P.H. Shipway, A study on the interaction between fretting wear and cyclic plasticity for Ti-6Al-4V. *Wear* 267 (2009) 270-282.
- [34] J. Jiaren, R.D. Arnell, T. Jin, The effect of substrate properties on tribological behaviour of composite DLC coatings. *Tribology International* 30 (1997) 613-625.
- [35] J. Takadoum, H.H. Bennani, M. Allouard, Friction and wear characteristics of TiN, TiCN acid diamond-like carbon films. *Surf. Coat. Technol.* 88 (1997) 232-238.
- [36] M. Shima, J. Okado, I.R. McColl, R.B. Waterhouse, T. Hasegawa, M. Kasaya, The influence of substrate material and hardness on the fretting behaviour of TiN. *Wear* 225-229 (1999) 38-45.
- [37] S. Fouvry, P. Kapsa, H. Zahouani, L. Vincent, Wear analysis in fretting of hard coatings through a dissipated energy concept. *Wear* 203-204 (1997) 393-403.
- [38] S. Fouvry, T. Liskiewicz, C. Paulin, A global-local wear approach to quantify the contact endurance under reciprocating-fretting sliding conditions. *Wear* 263 (2007) 518-531.
- [39] J. Ding, I.R. McColl, S.B. Leen, P.H. Shipway, A finite element based approach to simulating the effects of debris on fretting wear. *Wear* 263 (2007) 481-491.
- [40] J. Ding, S.B. Leen, E.J. Williams, P.H. Shipway, A multi-scale model for fretting wear with oxidation-debris effects. *Proc. Inst. Mech. Eng. Part J.-J. Eng. Tribol.* 223 (2009) 1019-1031.
- [41] N.M. Everitt, J. Ding, G. Bandak, P.H. Shipway, S.B. Leen, E.J. Williams, Characterisation of fretting-induced wear debris for Ti-6Al-4V. *Wear* 267 (2009) 283-291.
- [42] T. Liskiewicz, S. Fouvry, B. Wendler, Development of a Wohler-like approach to quantify the Ti(CxNy) coatings durability under oscillating sliding conditions. *Wear* 259 (2005) 835-841.
- [43] S. Fouvry, V. Fridrici, C. Langlade, P. Kapsa, L. Vincent, Palliatives in fretting: A dynamical approach. *Tribology International* 39 (2006) 1005-1015.
- [44] P. Bansal, P.H. Shipway, S.B. Leen, Finite element modelling of the fracture behaviour of brittle coatings. *Surface and Coatings Technology* 200 (2006) 5318-5327.

Figure 1

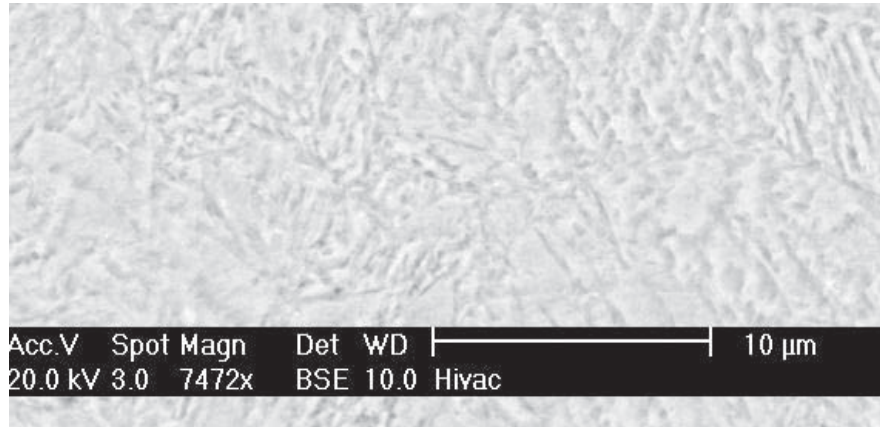


Fig. 1: SEM image of SCMV microstructure.

Figure 2

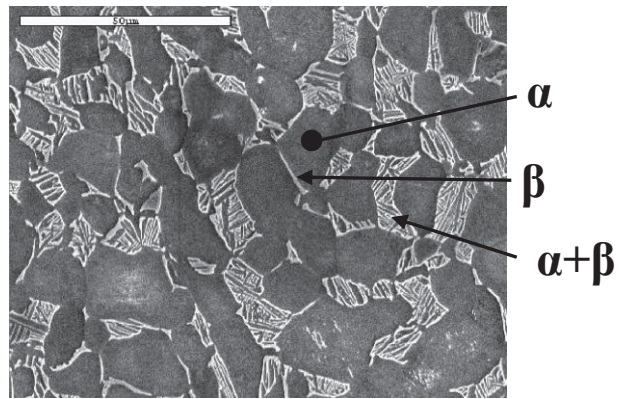


Fig. 2: SEM image of Ti-6Al-4V microstructure.

Figure 3

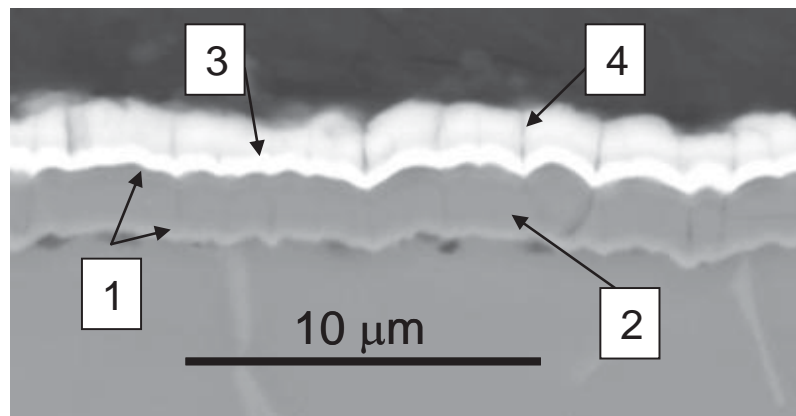


Fig. 3: SEM-BEI image showing BALINIT[®] C STAR coating in cross-section. (1) high chromium concentration, (2) chromium nitride, (3) high tungsten concentration, (4) tungsten/carbon.

Figure 4

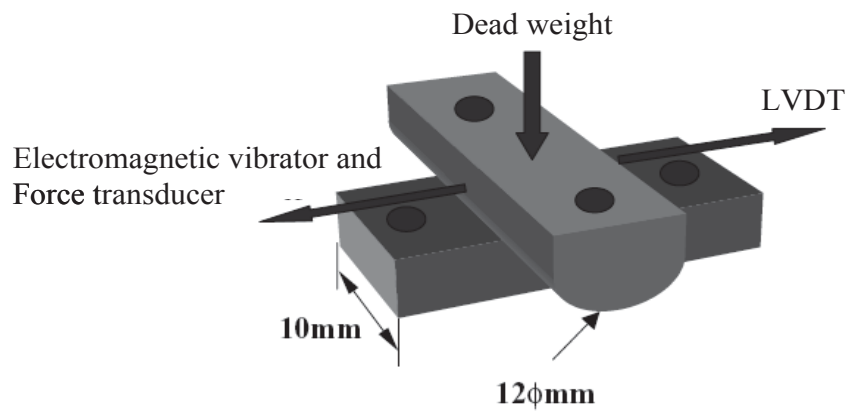


Fig. 4: Schematic of crossed cylinder-on-flat geometry used for fretting tests.

Figure 5

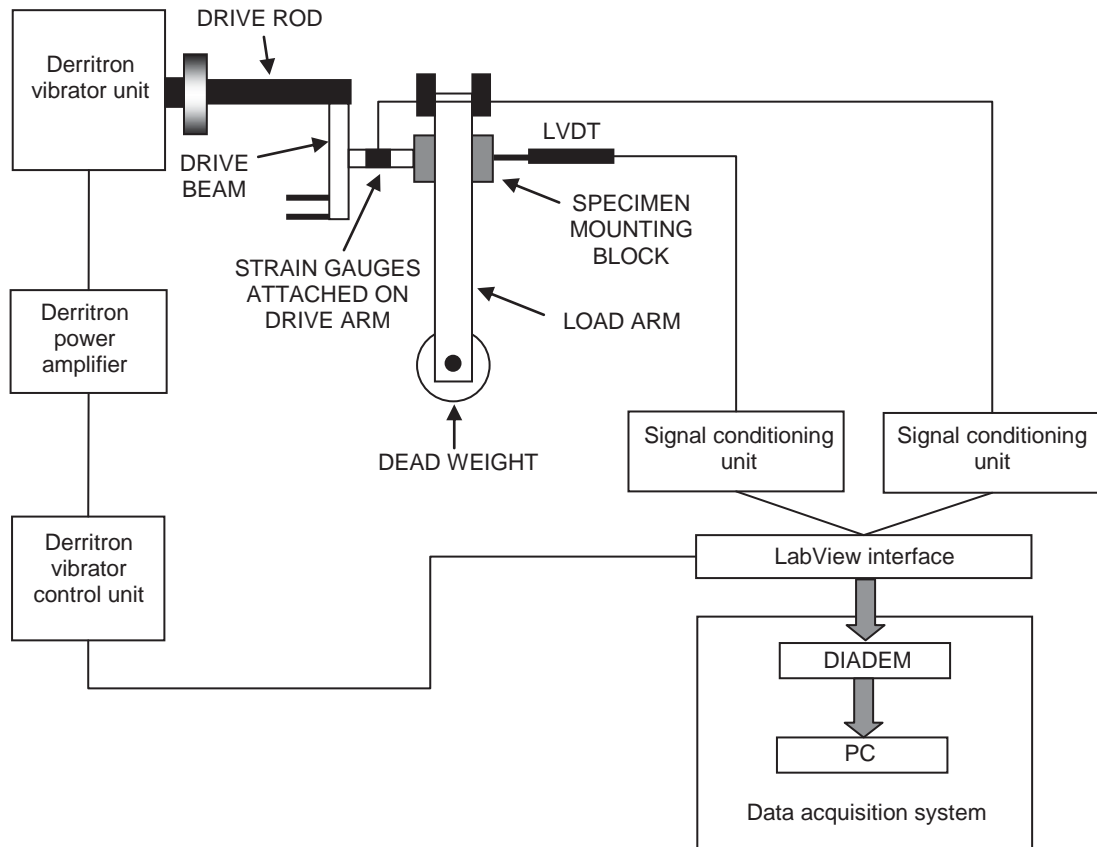
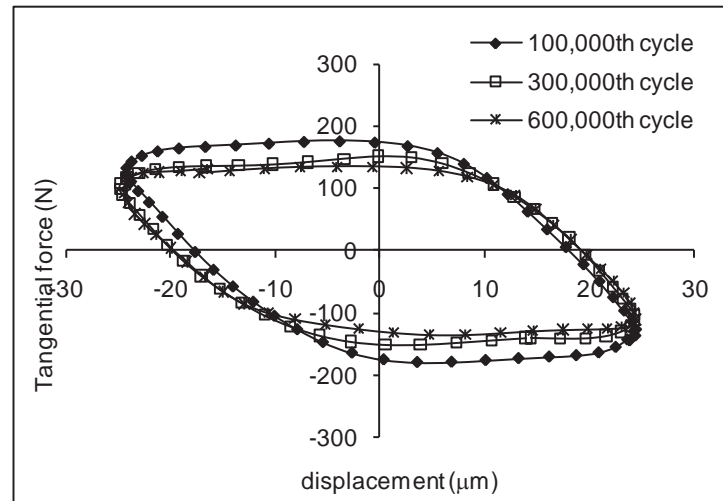
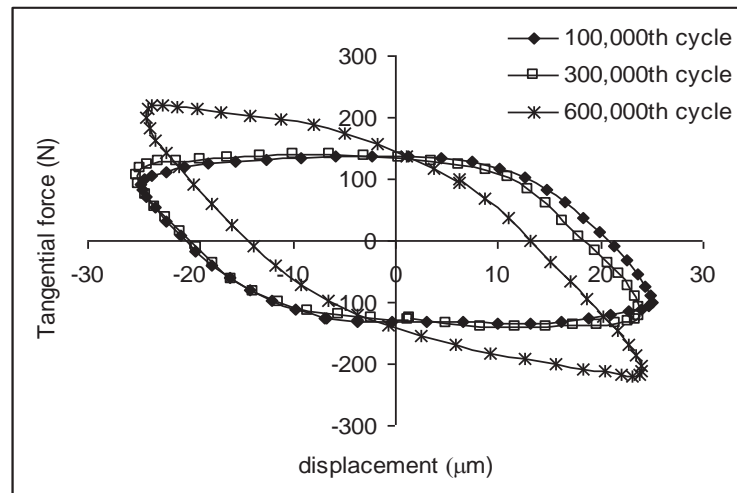


Fig. 5: Schematic diagram of fretting test rig arrangement.

Figure 6



(a)



(b)

Fig. 6: Hysteresis loops evolution of (a) coated SCMV pair for fretting test up to 600,000 cycles, and (b) coated Ti-6Al-4V pair for fretting test up to 600,000 cycles ($P = 500 \text{ N}$ and $2\delta_{app} = 50 \mu\text{m}$).

Figure 7

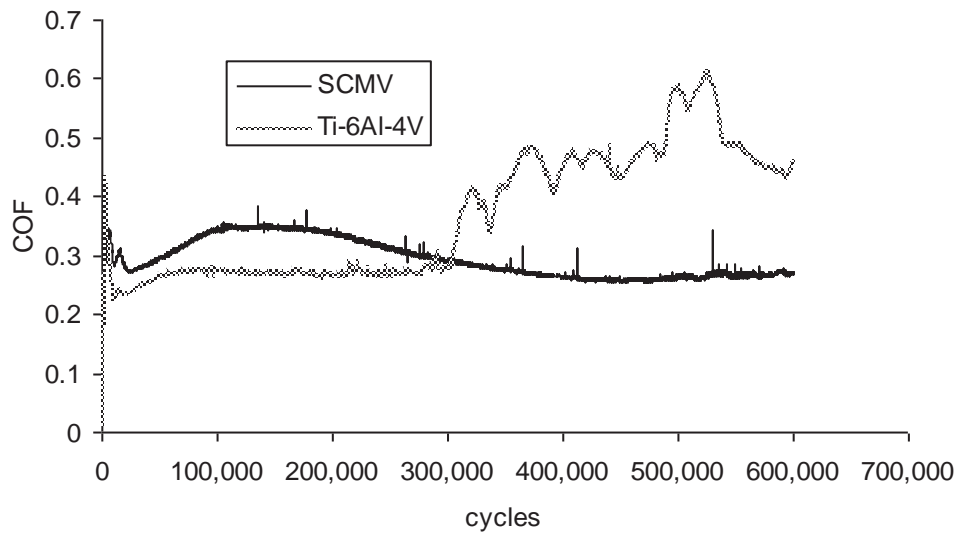
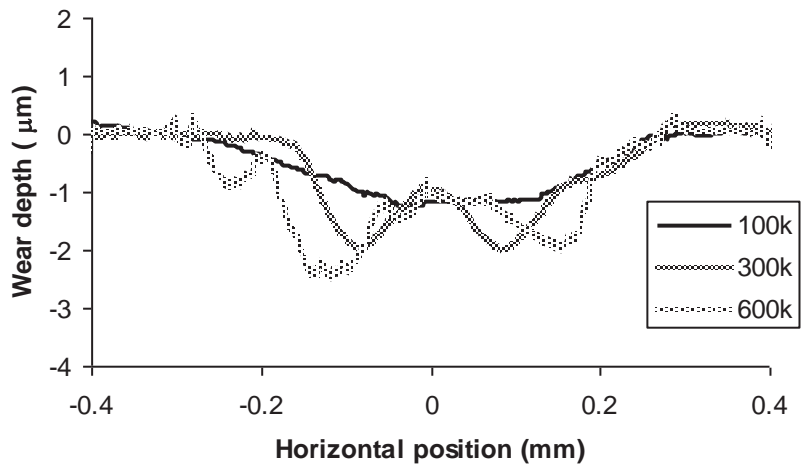
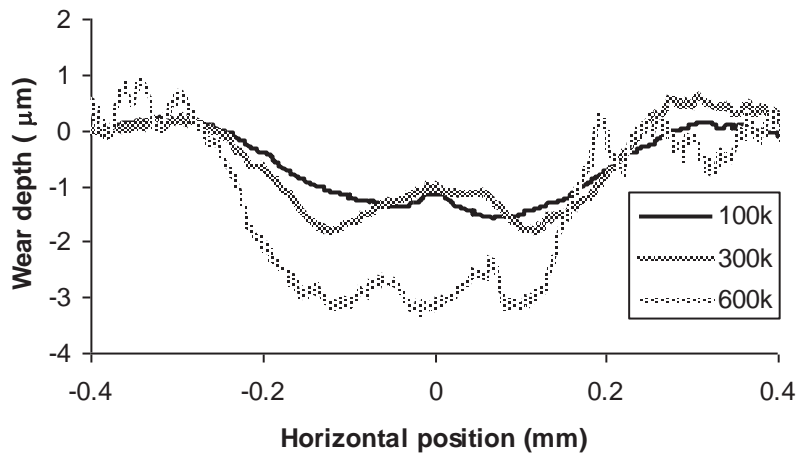


Fig. 7: COF evolution with number of fretting cycles for coated SCMV and Ti-6Al-4V pairs for tests up to 600,000 cycles ($P = 500$ N and $2\delta_{app} = 50$ μ m).

Figure 8



(a)



(b)

Fig. 8: 2-D measured average wear profile after 100,000, 300,000, and 600,000 cycles fretting test for coated (a) SCMV pair, and (b) Ti-6Al-4V pair ($P = 500$ N and $2\delta_{app} = 50$ μm).

Figure 9

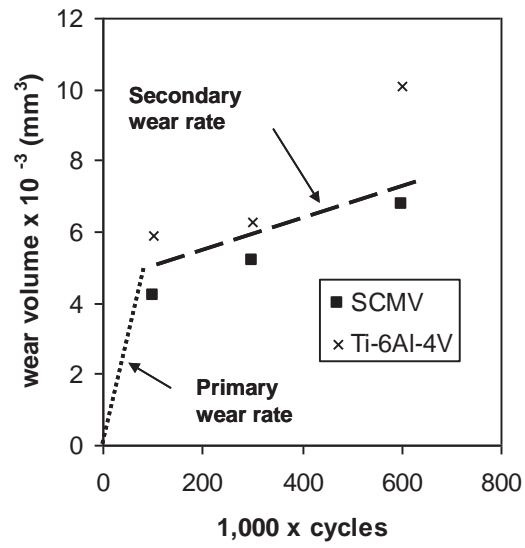


Fig. 9: Measured wear volume for coated SCMV and Ti-6Al-4V pairs showing two wear behaviour regime: primary wear rate and secondary wear rate ($P = 500$ N and $2\delta_{app} = 50$ μ m).

Figure 10

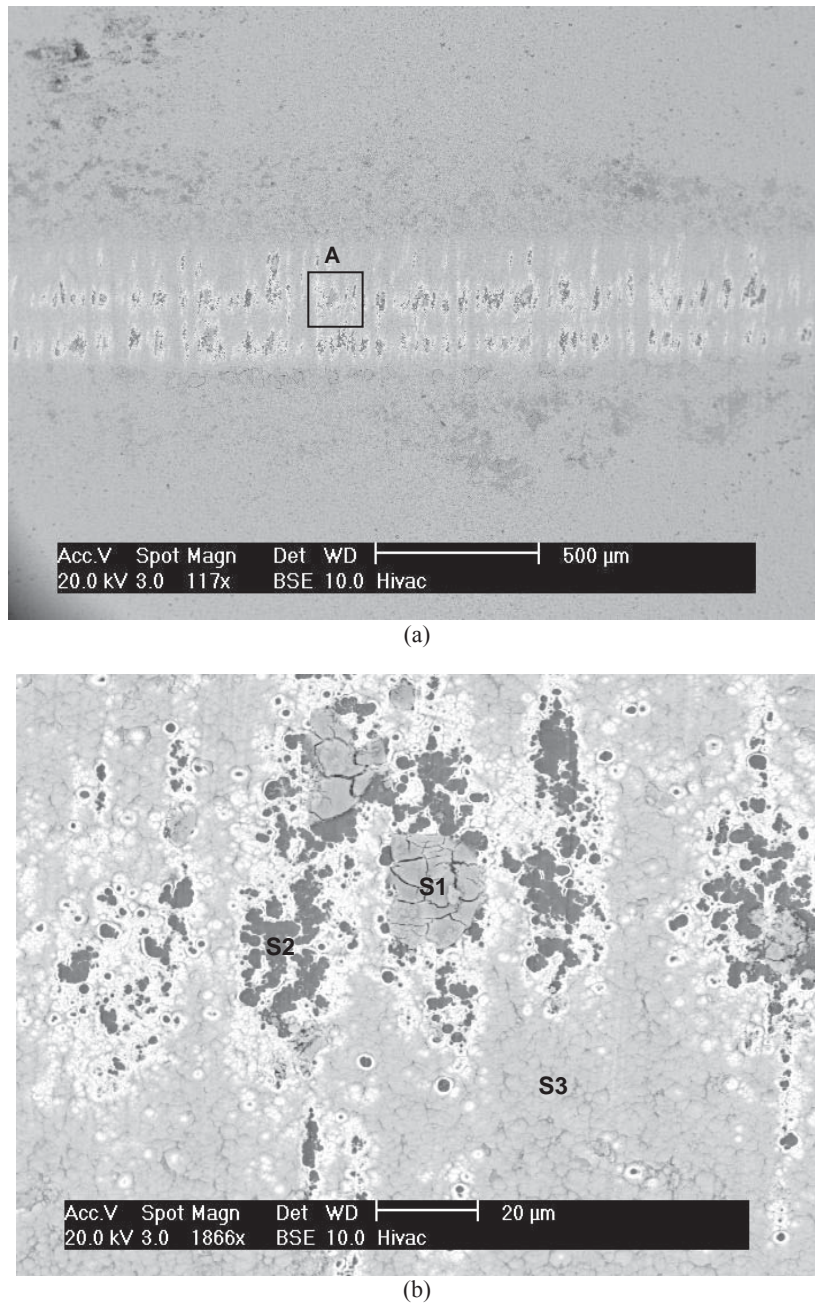


Fig. 10: SEM-BEI images of the wear scar for coated SCMV pair at the end of 300,000 cycles: (a) plan-view image, and (b) higher magnification of location 'A' showing the locations S1, S2 and S3 of EDX analyses ($P = 500$ N and $2\delta_{app} = 50$ μ m).

Figure 11

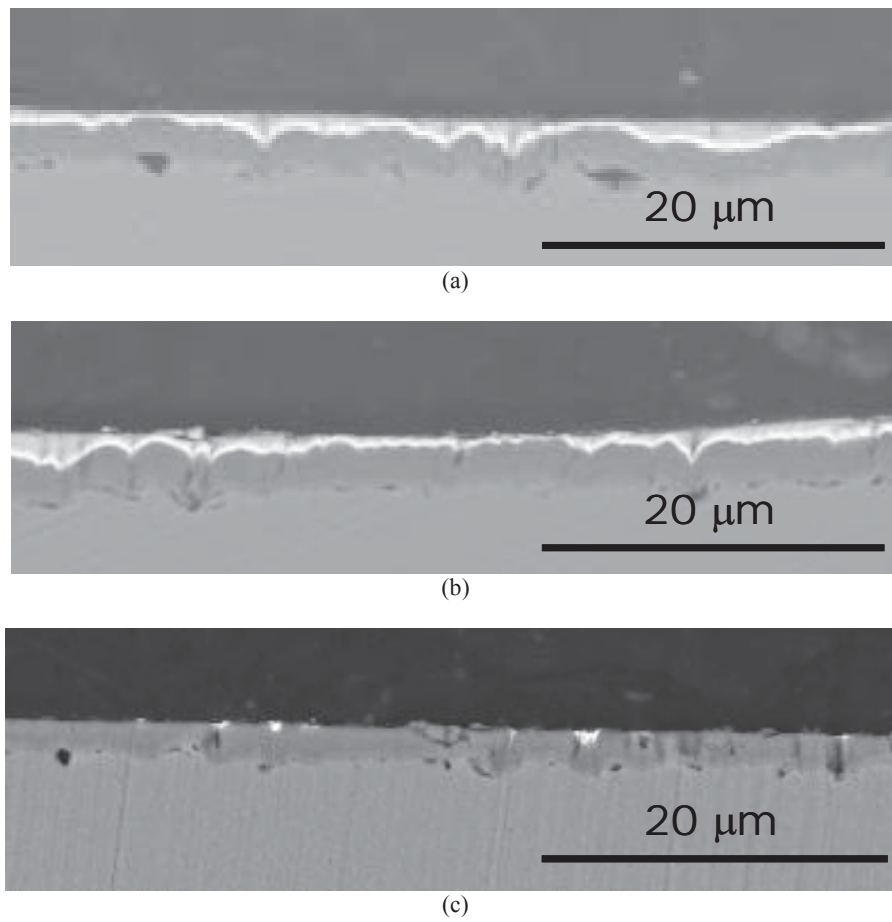
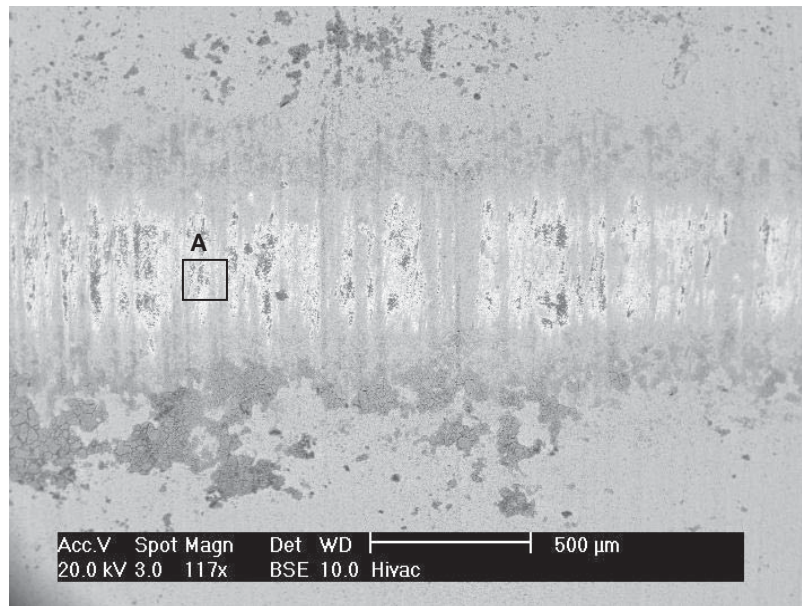
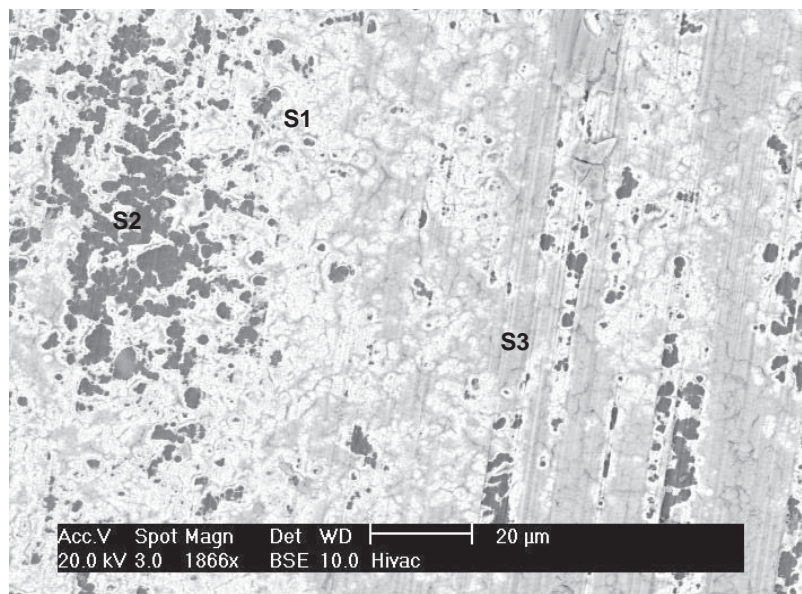


Fig. 11: SEM-BEI images of the wear scar cross-section for coated SCMV pair at the location of maximum wear depth at the end of (a) 100,000 cycles, (b) 300,000 cycles, and (c) 600,000 cycles ($P = 500$ N and $2\delta_{app} = 50$ μm).

Figure 12



(a)



(b)

Fig. 12: SEM-BEI images of the wear scar for coated Ti-6Al-4V pair at the end of 300,000 cycles: (a) plan-view image, and (b) higher magnification of location 'A' showing the locations S1, S2 and S3 of EDX analyses ($P = 500$ N and $2\delta_{app} = 50$ μm).

Figure 13

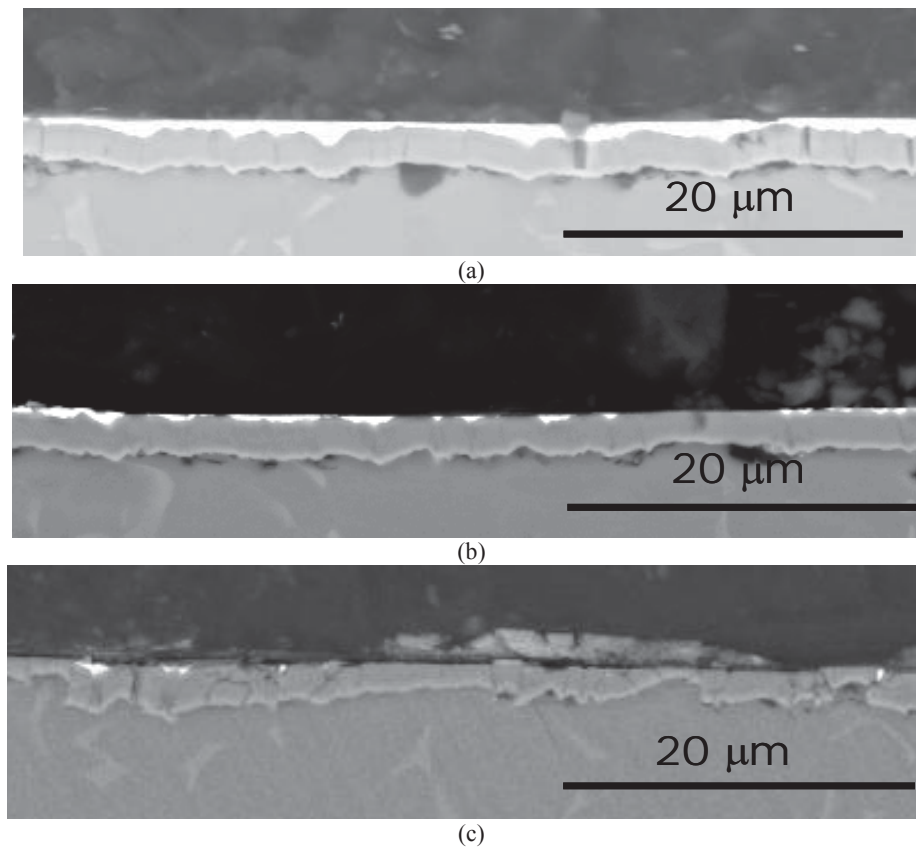


Fig. 13: SEM-BEI images of the wear scar cross-section for coated Ti-6Al-4V pair at the location of maximum wear depth at the end of (a) 100,000 cycles, (b) 300,000 cycles, and (c) 600,000 cycles ($P = 500$ N and $2\delta_{app} = 50$ μm).

Figure 14

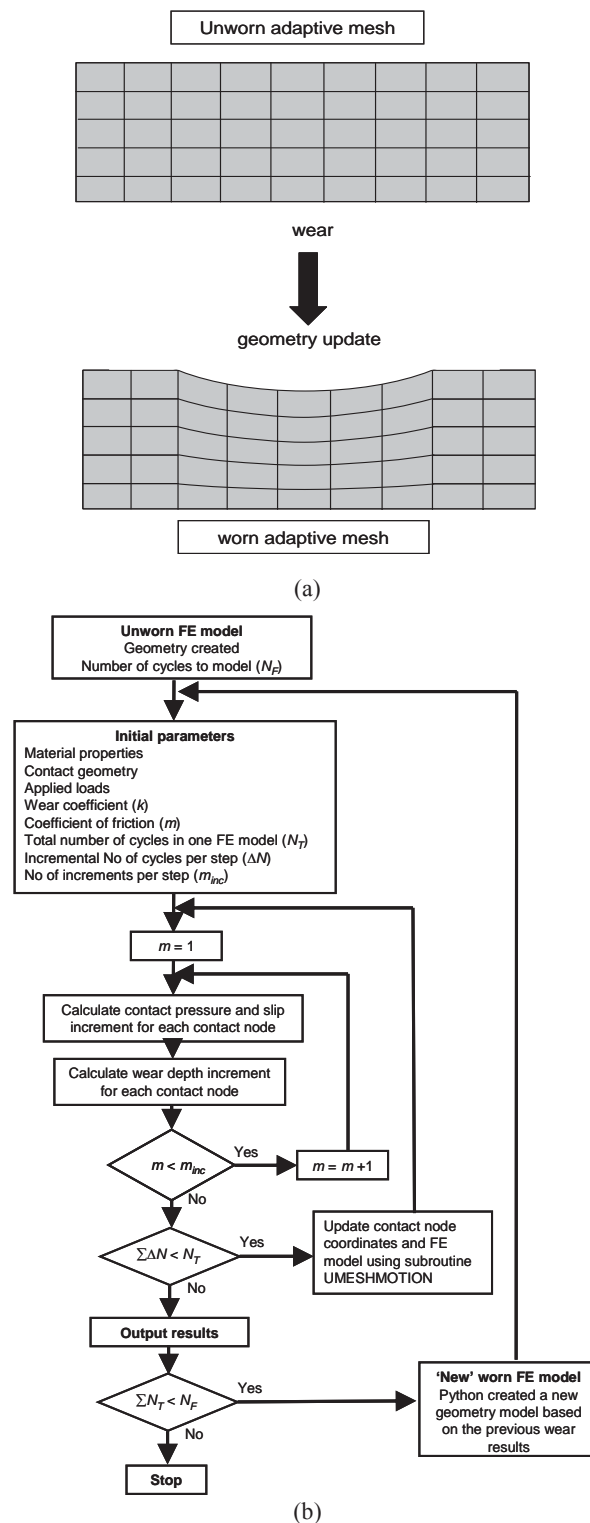


Fig. 14: (a) Schematic view of incremental wear depth on coating thickness and (b) flowchart illustrating FE-based incremental wear simulation methodology implemented in ABAQUS.

Figure 15

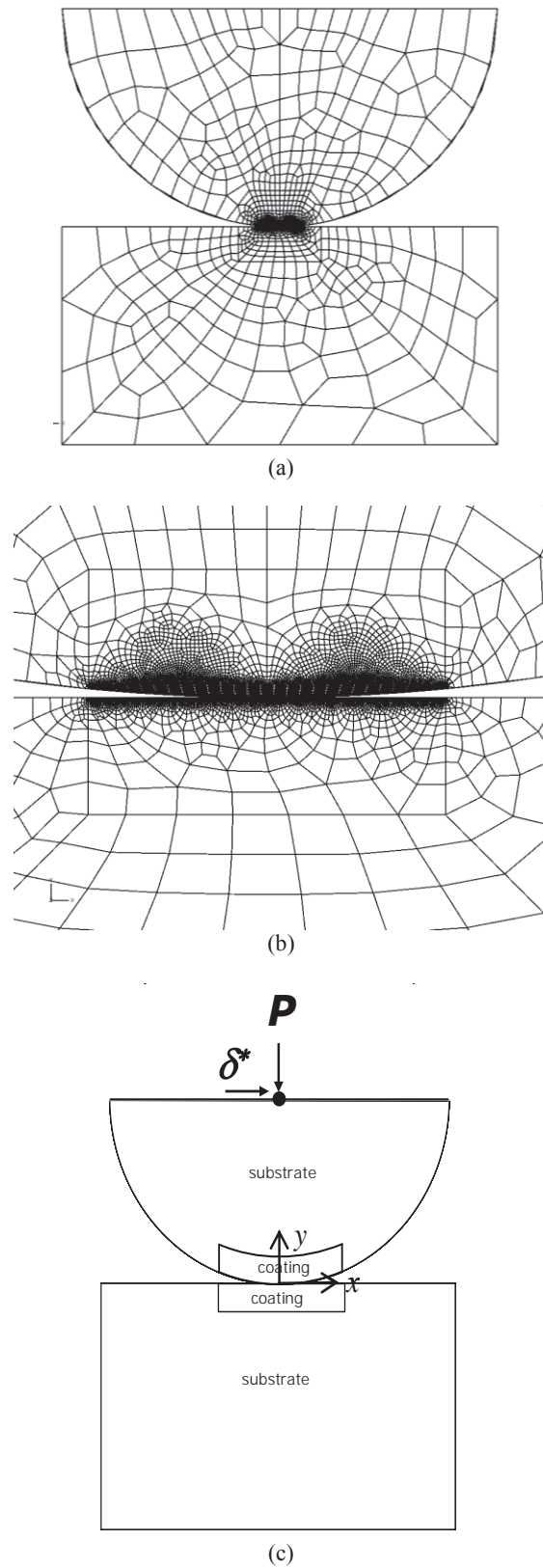


Fig. 15: (a) Full model mesh, (b) contact region mesh detail and (c) schematic view of the cylinder on flat coated substrate model.

Figure 16

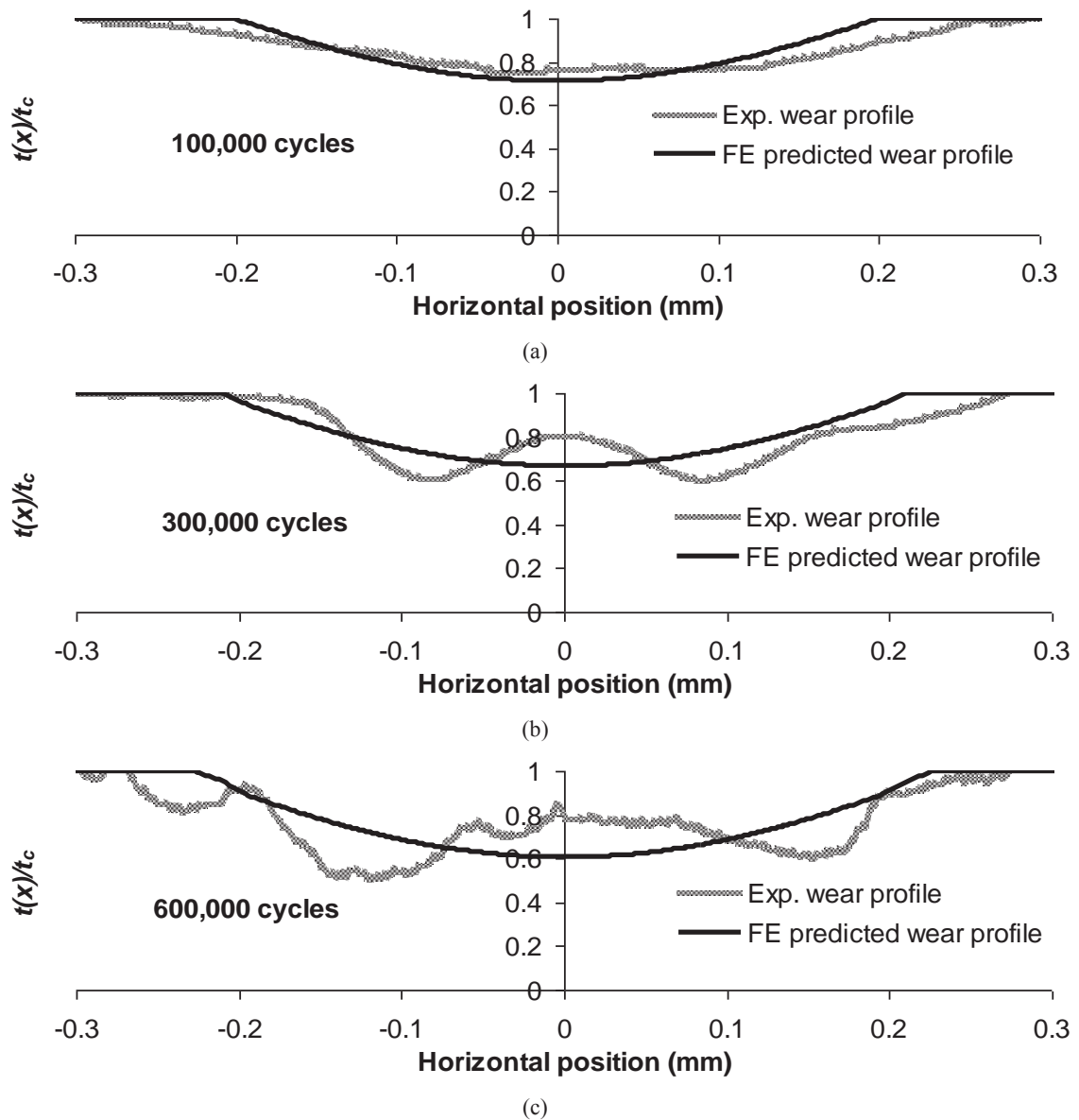


Fig. 16: Comparison of FE-predicted and experimental wear profiles for coated SCM pair for (a) 100,000 cycles, (b) 300,000 cycles, and (c) 600,000 cycles.

Figure 17

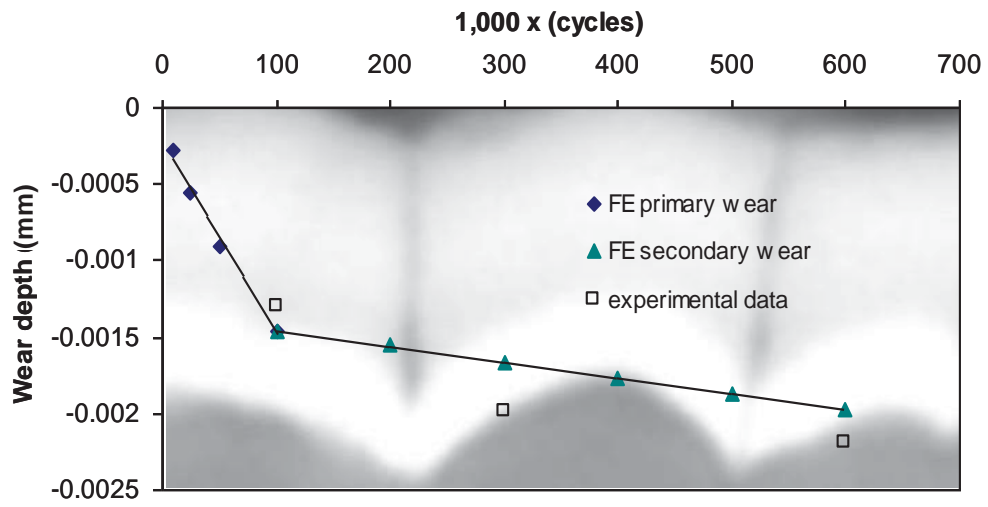


Fig. 17: Comparison of FE-predicted and experimental maximum wear depth superimposed with original coating cross-section image for coated SCMV pair presented up to 600,000 cycles.

Figure 18

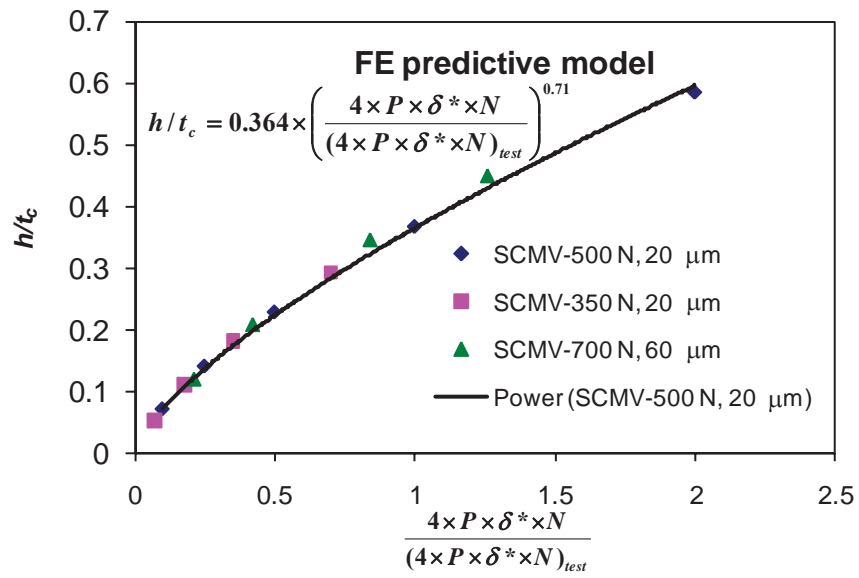


Fig. 18: FE-Predicted wear depth for other normal load and displacement combination.

Table 1

Table 1: Measured chemical composition of SCMV steel (measured by Optical Emission Spectroscopy).

Alloying Element	Composition (wt %)
C	0.36 - 0.38
Fe	Balance
P	≤ 0.003
S	≤ 0.003
Si	0.35 - 0.37
Ni	0.27 – 0.34
Cr	3.06– 3.09
Mo	0.90 - 0.93
As	≤ 0.005
Sb	≤ 0.003
Sn	0.003 – 0.005
V	0.22 - 0.23

Table 2

Table 2: Measured chemical composition of Ti-6Al-4V (measured by Optical Emission Spectroscopy).

Alloying Element	Composition (wt %)
Ti	Balance
Si	≤ 0.01
Mn	0.009 – 0.012
Cr	0.010 – 0.012
Mo	≤ 0.01
Al	6.29 – 6.43
Cu	≤ 0.01
Fe	0.15– 0.16
V	4.05 – 4.11
Zr	≤ 0.01
Sn	< 0.05
Nb	0.27 - 0.37
Pd	< 0.02

Table 3

Table 3: Fretting test conditions.

Normal Load, P (N/mm)	50.0
Stroke, $2\delta_{app}$ (μm)	50.0
Duration, N (num. of cycles)	100,000, 300,000, 600,000
Frequency (Hz)	20.0
Room Temperature ($^{\circ}\text{C}$)	14 – 22 (ambient)
Relative Humidity (%)	29-66 (ambient)